STUDENTS DESIGNING A HYDROGEN-POWERED UAV: A FLYING TEST BENCH FOR LIGHTWEIGHT ENERGY SYSTEMS

A. van der Heiden[*§], M. Willke[†§], J. Beckmann[‡§], N. Steveker[*§],
F. Stährfeldt[†§], J. Mellmann[†§], F. W. Fritsch[‡§], P. Nachtigal[*§], D. Mimic[*§¶]

[*] Institute of Turbomachinery and Fluid Dynamics, Leibniz University Hannover
An der Universität 1, 30823 Garbsen, Germany

[†] Institute of Thermodynamics, Leibniz University Hannover
An der Universität 1, 30823 Garbsen, Germany

[‡] Institute of Electric Power Systems, Leibniz University Hannover
Appelstraße 9a, 30167 Hannover, Germany

[§] Dynamics of Energy Conversion, Leibniz University Hannover
An der Universität 1, 30823 Garbsen, Germany

[¶] Cluster of Excellence SE^{2}A – Sustainable and Energy Efficient Aviation, TU Braunschweig
Universitätsplatz 2, 38106 Braunschweig, Germany

Abstract

The transition towards sustainable aviation requires technological innovation, skilled engineers, and societal acceptance of these new technologies – especially in the field of airborne hydrogen-powered energy systems. All three aspects benefit from introducing engineering students early to the opportunities and challenges associated with this field.

In this context, engineering students at Leibniz University Hannover conceive and design an unmanned aerial vehicle (UAV) which shall serve as a flying test bench for lightweight energy systems. Current test setups include a fully battery-powered and a fuel cell-based energy system. This paper presents the concept and design of a hexacopter, as well as the design and modelling of both a purely battery-powered and fuel cell-based energy system.

Keywords

Unmanned aerial vehicle; Fuel cell; Hydrogen

NOMENCLATURE

Symbols

e_m	gravimetric energy density	Wh/kg
I_cell	cell current	A
$\dot{m}_{\mathrm{H_2}}$	hydrogen mass-flow rate	g/h
$M_{\mathrm{H_2}}$	molar mass of hydrogen	g/mol
$\dot{n}_{\mathrm{H_2}}$	molar flow rate of hydrogen	mol
p	pressure	N/m^2
P_cell	cell power	W
p_m	gravimetric power density	W/kg
R_m	molar gas constant	J/(K·mol)
T	temperature	K
T_cell	cell temperature	K
t_flight	flight time	h
U_cell	cell voltage	V
$\dot{V}$	volume-flow rate	l/h
v	air velocity	m/s

Abbreviations

CAD	computer-aided design	
CFRP	carbon-fibre-reinforced polymers	
DMFC	direct methanol membrane fuel cell	
LiPo	lithium-ion polymer	
MTOM	max. take-off mass	kg
OCV	open circuit voltage	V
PEMFC	polymer electrolyte membrane fuel cell	
SOC	state of charge	
SOFC	soldie oxide fuel cell	
UAV	unmanned aerial vehicle	

doi: 10.25967/610219

INTRODUCTION

Current trends towards sustainable aviation, such as battery-electric, fuel cell-based, or hybrid-electric energy systems, are characterised by a significant increase in technological diversity compared to conventional architectures. Naturally, a successful transition is contingent upon three prerequisites.

1) Technological maturity: suitable technologies must achieve sufficient maturity for entry into service.
2) Qualified engineers: specialised skills are required for the design, operation, maintenance, and improvement of these technologies.
3) Societal acceptance: passengers must have sufficient confidence in these novel technologies.

While the quest for technological maturity of alternative energy systems is an active research topic, a proactive introduction of corresponding contents into engineering curricula seems expedient in order to promote the training of qualified personnel. Due to the wide variety of possible energy-system architectures and the interdisciplinary technological challenges often associated with it, it seems advisable to supplement theoretical foundations with practical, application-oriented engineering projects. These projects should acquaint students with the opportunities and challenges of sustainable aviation, familiarise them with the necessary methodical skills, and foster interdisciplinary thinking and creativity.

Practical application

An engineering project in which students design, build, and test a hydrogen-powered unmanned aerial vehicle (UAV) was introduced at Leibniz University Hannover, with the intention of developing useful skills in the context of energy systems for sustainable aviation.

The project task was selected based on the following criteria.

1) The problem must be related to the target application, in order to provide a clear motivation.
2) The core problem to be solved within the project must capture the core engineering challenge or design conflict of a given application.
3) The problem must be manageable. This implies that complexity, which is unnecessary for achieving the teaching objective, should be removed.
4) The problem must be attractive, in order to capture the attention of students (and possibly the general public).

The core problem approached in this project is the design of a climate-friendly, lightweight energy system, which maximises the flight time and payload-capacity of a given flying device. The airborne application shifts the focus from mere component-specific efficiency considerations to the very tangible targets of increasing the achievable flight time and load capacity. The problem addresses the core challenges of achieving a sufficient power and energy density. In this context, the flying device is to be considered a flying test bench rather than a vehicle. This implies that the selection of a device type should be based on its simplicity and feasibility within a student project rather than on its flight performance. Multicopter UAVs satisfy this requirement, especially for study programmes without dedicated courses in aircraft design. The familiarisation with novel technologies, e.g., hydrogen-based energy systems in aviation, may also promote their societal acceptance—especially if the project is advertised publicly, e.g., through regional or national news outlets.

Objective and organisation

The project goal is the design of a UAV which serves as a flying test bench for a hydrogen-powered, fuel cell-based energy system. The UAV should achieve a payload capacity of 5 kg, a flight duration of 60 min, and allow hovering. The project members are subdivided into several teams, which conduct the preliminary and final design of the UAV, of the energy-system architecture, and of the fuel-cell subsystem, as well as the manufacturing, assembly, and testing of the UAV.

Structure of this paper

This paper presents the design methodology of for a UAV with a fuel cell-based energy-system architecture. An overview of the structure of this paper is provided below:

1) The first section presents a brief summary of relevant literature regarding UAVs, sizing, and resulting design of the flying test bench.
2) The second section introduces selection criteria for suitable fuel cells, and fuel-cell cooling.
3) The third section introduces the model-based design of the energy-system architecture.
4) Finally, the fourth section iterates the conclusions of this paper and provides an outlook on future flight experiments.

1. DESIGN OF THE FLYING TEST BENCH

1.1. Existing concepts

Unmanned aerial vehicles may be classified either as fixed-wing aircraft or rotorcraft. Fixed-wing UAV achieve higher speeds, whereas rotorcraft are capable of taking off and landing vertically, as well as hovering. Therefore, rotorcraft are more suitable for urban regions while fixed-wing UAVs tend to perform well for tasks such as observing large areas. [1]

Alternatively, UAVs may be classified with respect to their energy system. Most commonly, UAVs are powered by lithium-ion polymer (LiPo) batteries [2]. On the other hand, UAVs may be driven by a fuel cell-hybrid system. Table 1 provides an overview of several commercially available UAVs with both battery-based and fuel cell-based energy systems, together with relevant characteristics like the flight duration, maximum take-off mass (MTOM), and the payload capacity.

Manufacturer and UAV	Type	Propulsion system	MTOM in kg	Payload in kg	Flight duration in min
DJI Mavic 3 Pro [3]	Quadrocopter	LiPo	0.958	0	43
Yuneec H520 [4]	Hexacopter	LiPo	2.5	0.855	25-30
Doosan DS30W [5]	Octocopter	hydrogen	24.9	3	120
H3 Dynamics HyCopter [6]	Hexacopter	hydrogen	16.5	2.5	180
EnergyOR H2Quad 1000 [7]	Quadrocopter	hydrogen	10	1	120

TAB 1. Comparison of characteristics of available UAVs

While being non-exhaustive, Tab. 1 suggests that LiPo-driven UAVs tend to achieve lower flight durations than fuel cell-based systems. Furthermore, the latter achieve higher MTOMs and can transport heavier payloads. Apeland et al. [8] confirm this observation: the authors establish a relationship between the mass of the energy system and the endurance of the UAV. They conclude that a battery-powered energy system is more advantageous up to a mass of 7.3 kg. Above this mass, increasing the battery size is not sufficient to achieve higher endurances.

Battery-powered energy systems exhibit this limitation because the flight time of a multicopter is essentially determined by its power requirements and energy-storage capacity:

$$t_{\mathrm{flight}} = \frac{e_{\mathrm{m}}}{p_{\mathrm{m}}} \tag{1}$$

Increasing the energy-storage capacity of a battery increases its mass, which raises the power requirement. This, in turn, may limit the flight duration. [9]

For multicopters, the specific power requirement p_{m} is approximately 145 W/kg. The energy density e_{m} is approximately 180 Wh/kg for lithium batteries [9]. Taking into account that the energy density of the entire multicopter is lower than the energy density of the battery, this results in a flight duration t_{flight} of a maximum of about one hour. Increasing the battery capacity leads to an increase in the power demand and thus not necessarily to an increase in flight time [9]. The relationship is shown in Figure 1. For a small ratio of battery mass to empty mass, the flight time can be increased by using a larger battery. However, the slope decreases towards larger ratios of the batteries to the empty mass.

In contrast, fuel cell-hybrid energy systems are capable of achieving longer flight durations. Due to the significantly higher energy density of hydrogen compared to that of a LiPo battery, the energy storage (tank) is much more scalable with almost unchanged power requirements despite considerable efficiency disadvantages in the conversion of hydrogen into electrical energy.

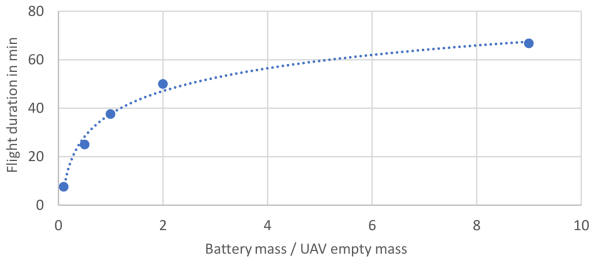

FIG 1. Limited flight time for battery-electric flying. A larger battery does not always increase the flight time (data from [9]).

1.2. UAV sizing and design

Initially, concepts of both a hexacopter and octocopter with coaxial rotors were examined concurrently (see Fig. 2). The hexacopter which will be discussed below was selected due to an increased redundancy of the rotors and due to its lower estimated overall mass.

FIG 2. Preliminary UAV design concepts; left: coaxial octocopter [10], right: hexacopter [11]

The initial sizing of the UAV chassis, motors, and fuel cell was conducted in tandem, based on existing data of commercially available devices. The fuel-cell sizing is described in greater detail in section 2. A computer-aided design (CAD) model was set up subsequently, in order to obtain more accurate mass estimations.

A parametrisation of the CAD model allows an iterative re-scaling of the model, which may be necessary if a re-sizing of the energy system is required. This was, however, not necessary in this case. The final design achieves an expected empty mass of approximately 19 kg. The actual mass may differ slightly, due to the uncertainty in the estimated mass of the hydrogen tube and electric cables. The resulting design is shown in Fig. 3

To enable both a controlled descent at empty mass and a rapid climb at MTOM, a motor–rotor combination, which covers a correspondingly wide thrust spectrum, must be selected. Six motor–rotor units consisting of a T-Motor Antigravity MN8012 electric motor and a T-Motor 28"×9.2" rotor each can generate a total thrust in the range of 98 to 560 N [12], which is considered sufficient for the present requirements.

The UAV is subdivided into four assemblies: the motor–rotor unit, the boom frame, the lower central

unit and the upper central unit. An important aspect of the design of the UAV is the modularity of the assemblies. This facilitates, among other things, future modifications of the power system.
The lower central unit comprises the landing skids and is used to mount the energy system consisting of the fuel cell and the LiPo batteries. Furthermore, this assembly carries the payload. Conversion to a pure battery-electric energy system is thus easily possible. The upper central unit carries the hydrogen tank and most of the board electronics. Tanks of different sizes can be mounted, depending on the target mission.
Three main materials are used for the chassis of the UAV: carbon-fibre-reinforced polymers (CFRP), EN AW 7075 aluminium, and plastic (VeroWhite Plus) for 3D printed parts.
The structural strength of the UAV design was examined by means of a finite element analysis (FEA). However, for critical components, the results of the FEA will be validated experimentally before conducting flight tests.

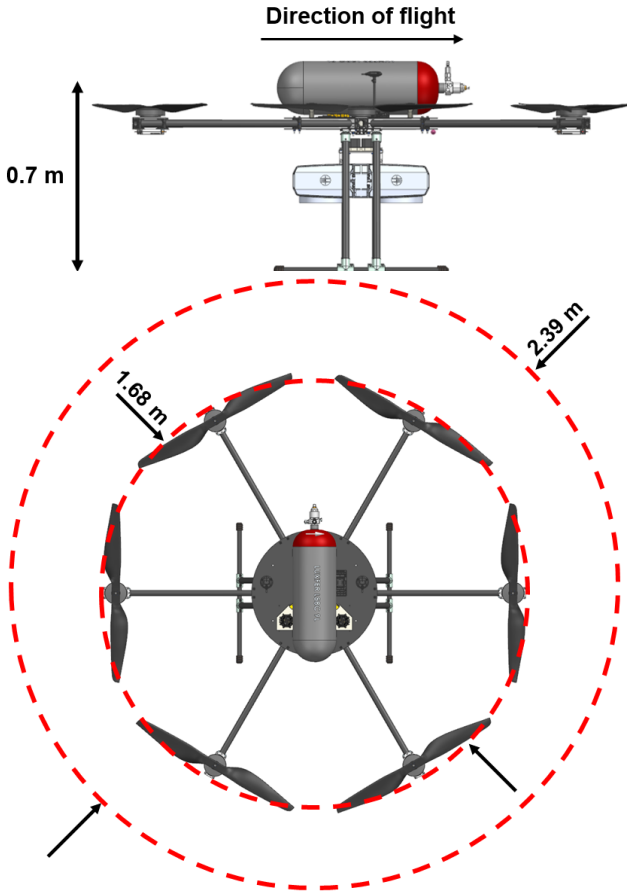

FIG 3. Final design of the UAV

2. SELECTION OF A SUITABLE FUEL CELL

2.1. Fuel-cell types

There are three established types of fuel cells for UAV applications: polymer electrolyte membrane fuel cells (PEMFC), solid oxide fuel cells (SOFC) and direct methanol fuel cells (DMFC) [13]. The most common type is PEMFC, since it achieves high power densities and adjusts well to load fluctuations. Furthermore, the start-up time is short, due to the operation at near-ambient temperatures. The major disadvantage of PEMFCs are the high cost of the membrane and the noble-metal catalyst. SOFCs have a very high operating temperature of 600 to 1000 °C, which facilitates high reaction rates without the use of expensive catalysts. However, this also results in a long start-up time for the fuel cell and a complex thermal management, especially for small-sized fuel cells. DMFCs can be used with liquid methanol which has a higher energy density and is easier to handle, compared to a compressed gas. However, this types suffers from low power densities and energy-conversion efficiencies, which negates the advantage of the high energy-density fuel in terms of overall system mass [14, 15].
Due to their low power densities, long start-up times, and poor transient characteristics, SOFCs and DMFCs are not an attractive option for multicopter UAVs. In fixed-wing UAVs, they might better exploit their advantages, due to the more continuous load profiles. In summary, PEMFCs seem to be the most suitable option for the application in multicopter UAVs and will be discussed below [14].

2.2. Fuel-cell suppliers

There are several manufacturers on the market, which offer fuel cells specifically for the use in UAVs. Table 2 lists the most relevant models on the market in the rated power range from 1 kW to 3 kW. The fuel-cell systems comprises an integrated balance-of-plant, such as DC/DC converters, fans, pressure regulating valves, and controllers. The systems are designed to be lightweight, which is crucial for the flight performance of the UAV.

Manufacturer	Product	Rated Power in kW	Weight in kg	Specific Power in W/kg
Doosan [16]	DP30M2S	2.7	6.9	391
H3 Dynamics [17]	A-1200 (HV)	1.2	2.1	571
	A-2000	2	3	667
Honeywell Aerospace [18]	1200U	1.2	4	300
Intelligent Energy [19]	IE-SOAR 1.2	1.2	2.1	444
	IE-SOAR 2.4	2.4	4.8	500
Spectronik [20]	Protium-1000	1	4.8	208
	Protium-1500	1.5	6.35	236
	Protium-2000	2	7.69	260

TAB 2. A selection of fuel-cell systems with a rated power range from 1 kW to 3 kW

2.3. Fuel-cell sizing

The design of the fuel-cell system depends on the desired application of the UAV. An overview of the design methods for different use cases is depicted in [21]. The sizing process is iterative, since the sizing of the UAV influences the power consumption, which determines the sizing of the energy system, which in turn affects the mass of the UAV. The power consumption while hovering can be roughly estimated by the relationship between the power and thrust of the motors (see Fig. 4). In this case, the hovering power for an empty mass of 20 kg and an MTOM of 25 kg is estimated to be 1.84 kW and 2.51 kW, respectively.

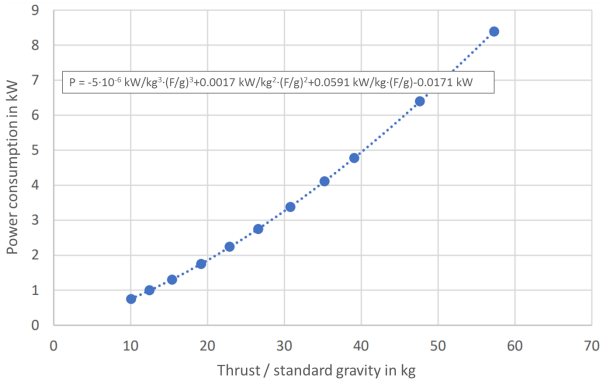

FIG 4. Ratio between thrust and power consumption of the six T-Motor Antigravity MN8012 (data from [12])

Based on this estimation, the fuel-cell system IE-SOAR 2.4 by Intelligent Energy [19] was selected since it fulfils the power demand whilst exhibiting a high power density. It has a nominal power of 2.4 kW and a peak power of 3.2 kW; it is equipped with a fan that supplies the stack with ambient air, which is used for both oxygen supply and cooling. The fuel-cell system includes a cylindrical 9 l Type 3 hydrogen tank which can be filled up to 300 bar. Figure 5 depicts the structure of the fuel-cell system.

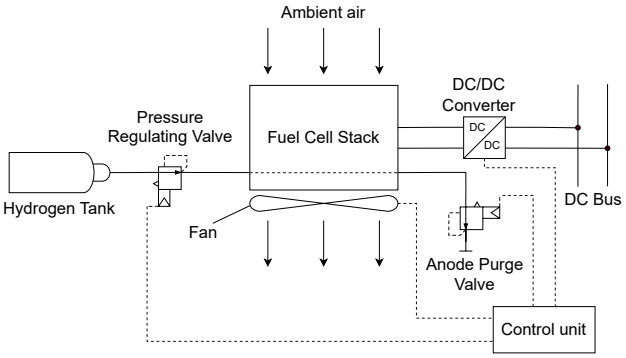

FIG 5. Schematic of the Intelligent Energy IE-SOAR fuel-cell system

Considering a constant operation at 2.4 kW, the stack has a hydrogen consumption of 160-190 g/h. Assuming the worst case of 190 g/h, a cylinder pressure of 300 bar and a gas temperature of 20 °C, the minimum tank volume per hour of flight time equates to

$$\dot{V} = \frac{\dot{n}_{\mathrm{H_2}} R_{\mathrm{m}} T}{p} = \frac{\dot{m}_{\mathrm{H_2}} R_{\mathrm{m}} T}{M_{\mathrm{H_2}} p} = 7.657\,\mathrm{l/h}, \tag{2}$$

according to the ideal gas law. Thus, the 9 l tank is sufficient to operate the fuel cell-stack for approximately 1 hour and 10 minutes at nominal power. The actual power consumption and flight duration under real-world conditions will be investigated in future flight tests.

2.4. Fuel-cell cooling

In PEMFCs, hydrogen and oxygen react to form water, producing electrical energy. This reaction produces heat which raises the temperature inside the fuel cells. [15]
To sustain an efficient operation of PEMFCs, excess heat and produced water must be removed from the cells. This is important to avoid cell damage due to overheating or flooding in the cells. [22]
PEMFCs achieve thermodynamic efficiencies of up to 60% , which means that 60% of the internal chemical energy of the hydrogen are converted into electrical energy to drive the rotors of the UAV. [23]
The biggest part of the loss is excess heat. The amount of heat and water produced increases with the rate of reaction in the fuel cell, which necessitates a complex control of the cooling subsystem. [24]

Cooling methods for PEM fuel cells

One of the main influences on the performance of PEMFCs is the cooling method. It affects the operating temperature, water management, and contamination of the cells. [25]
There are three main methods of cooling fuel cells: air-cooling, liquid, and phase-change cooling. Most stationary PEMFC systems are cooled with a liquid coolant. Liquids have a high density and can provide efficient cooling of the cells. Hence, a liquid coolant needs more energy to circulate due to its higher density and viscosity than air. In comparison to air cooling systems, liquid and phase-change cooling systems are heavier due to the required coolant tanks and various additional components, like pumps and heat exchangers. [26]
Air cooling is therefore preferable for the use in multicopter UAVs because of its simplicity and low mass. All manufacturers listed in Tab. 2 rely on air cooling. Fuel-cell stacks with more than 1 kW power need additional air-cooling ducts to the cathode channels to increase the heat-removal capacity. [23]
Studies have shown that the position of the fan has a major impact on temperature uniformity and the speed of the airflow in the fuel cells. Moving the fan from the inlet to the outlet, in order to draw air through the fuel cells instead of blowing improves the temperature uni-

formity and may raise the overall stack performance by 16%. [27]

Humidification of the membranes

The membranes of PEMFCs must maintain a certain humidity for the ion transport to take place. The humidity washes away contaminants of the gases that can damage the membranes and lead to leaks between the gases. [28]
Still, high water content in the cells can lead to flooding, limiting the gas flow and the activity of the catalyst [29]. The starvation of the cell decreases its power and leads to temperature peaks in the non-flooded areas [30]. Local temperature peaks lead to platinum dissolution and carbon corrosion [31]. These effects cause irreversible degradation of the fuel cells and must be avoided or minimised by, i.a., a suitable cooling strategy.
Typically, the humidification of PEMFCs is done by an external humidifier that adds vaporised water to the reactant gases, mostly the air. These devices increase the mass and costs to the fuel-cell system [32]. Therefore, self-humidifying components are preferable in fuel cells for portable systems.

Flow-field designs

Parallel or serpentine flow-fields are the most common designs used for PEMFCs. Increasing the convection of the airflow in the cathode by a flow-field design with pin-shaped or bean-shaped flow patterns can improve the heat removal from the airflow compared to the parallel flow-fields. [33]
Another strategy is a cathode gas channel designed in a diffuser shape. The cross-sectional area of the cathode-gas channels increases gradually from the inlet to the outlet, and decreases for the cooling channels. The diffuser-type gas channel decelerates the flow continuously as it moves downstream. This helps the membrane to gain moisture from the water produced in the cell and decreases the water removal through the gas channel. On the other hand, the shape of the cooling channels accelerates the cooling air flow which allows a more effective waste heat removal. [24]

3. DESIGN OF THE ENERGY-SYSTEM ARCHITECTURE

3.1. Operating behaviour of hydrogen fuel cells in the system network

Fuel cells achieve the highest efficiency in part-load operation at low currents. The system efficiency is highest in the medium power range since the periphery for operating the fuel cell represents a non-negligible base load. In order to always operate the fuel cell in a range with high efficiency, an energy storage, for example in the form of a battery, is necessary. The storage unit can be charged when the power demand on the fuel cell is low. At the same time, the storage unit can support the fuel cell when high power is demanded and help to avoid operation in the inefficient full-load range. [34]
A smaller fuel cell in combination with a buffer battery can increase the system efficiency. If the take-off mass is reduced, this can have a positive effect on the flight time. When used in a multicopter, the following operating states can be distinguished [35]:
1) the fuel cell as sole energy supplier,
2) power addition by the fuel cell and battery, and
3) the fuel cell charges the battery when the power demand is low.

3.2. Lithium-ion storage systems for use in a multicopter

Battery-based storage systems differ primarily in terms of the technology used. Suitable types depend upon the intended application as it determines the required operational ranges with regards to, e.g., temperature, service life, or energy density [36]. The primary requirements for the battery of the multicopter are high gravimetric power and energy densities. Lithium-ion technology combines both properties with a comparatively long service life [36]. The highest energy density is achieved by systems made of lithium nickel cobalt aluminium (NCA) oxide and lithium nickel manganese cobalt (NMC) oxide [37]. The battery-cell shape also plays a decisive role for the energy density. The highest energy densities can be achieved by pouch cells. The advantages of this cell shape include high thermal conductivity, scalability, and compact packaging. The disadvantages include lower mechanical stability and tightness, and a possible “blow-up” due to increased internal pressure caused by gas generation. Prismatic and cylindrical cells have disadvantages in heat dissipation and packaging but are superior in terms of safety [38]. Pouch cells were selected for this work.

3.3. Models for simulating the buffer storage: isothermal energy model

An isothermal energy model [39] is used to determine the state-of-charge (SOC, describes the available capacity of a battery in relation to the nominal capacity) of a storage tank of given capacity by providing the power applied to the storage as a known input. Possible power and SOC limits are respected. The model takes into account a constant charging and discharge efficiency. The calculation is carried out with a discrete step size [39]. In contrast to a non-isothermal model, the isothermal model calculates the output values at the level of the entire storage unit or battery and not at the battery-cell level. The calculation is carried out in arbitrarily small equidistant time steps. The SOC of the battery is computed by calculating the power applied to it, taking into account the charging and discharging efficiency. The self-discharge of the battery during the flight is neglected, as this is in the range of 0.3 to 5% per month for LiPo batteries [40, 41]. In this

model, the fuel cell is considered as a source, which can both serve the load as well as charge the battery. The operating behaviour of the fuel cell is simulated in different ways:

a) instantaneous power change or without operation control,
b) delayed power change with specification of a delay by an arbitrary rate of power increase (limitation of the edge steepness),
c) via filtering by a moving-average filter,
d) with consideration of a humidification time for the fuel cell,
e) with halved power output of the fuel cell without operation control, and
f) a combination of b), c) and d).

Figure 6 shows exemplary output curves for the fuel cell and storage tank.

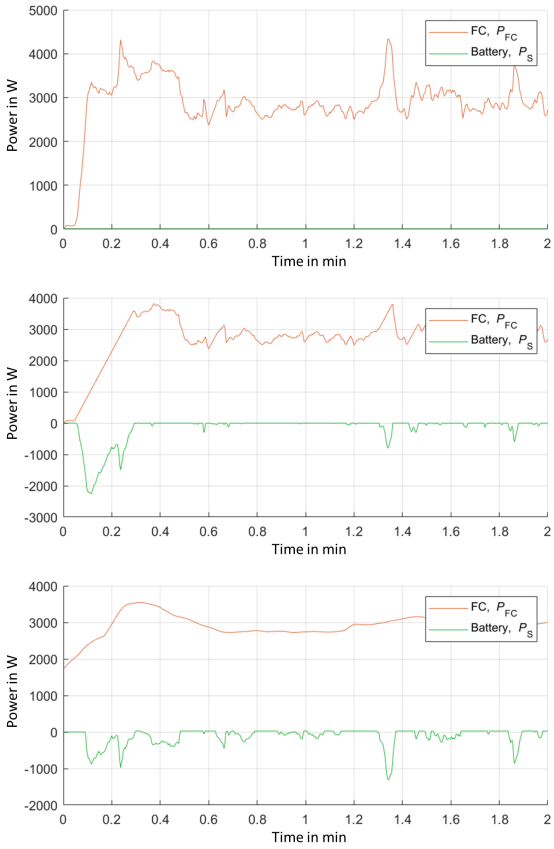

FIG 6. Instantaneous power change or without operation control (top); delayed power change with specification of a delay by an arbitrary rate of power increase (centre); moving-average filter (bottom)

Depending on the operating mode, different performance profiles can be defined for the fuel cell, which have a direct effect on the requirements for the battery. The signal filtered according to cases b) to f) is assigned to the fuel cell. The storage power is calculated using the difference between the original signal and the filtered signal. The isothermal energy model is based primarily on performance variables and contains few technology-specific parameters (such as a SOC-dependent charge/discharge efficiencies) [39]. The thermal behaviour of the battery is not taken into account.

3.4. Non-isothermal energy model

By using a non-isothermal model [42], a more exact simulation of the problem is possible, since it takes into account important technology-specific parameters. The state of the battery is calculated at the battery-cell level by means of a differential equation. The input variables for this are the SOC, the cell voltage, current, and temperature. The cell current is calculated from the applicable power and the cell voltage from the previous step:

$$I_{\mathrm{Cell}}(i) = \frac{P_{\mathrm{Cell}}(i)}{U_{\mathrm{Cell}}(i-1)}. \tag{3}$$

The state of charge is calculated from the capacity and the cell current. The differential equation is solved with an ode15s solver. The solution vector again consists of the state of charge, the cell voltage, the cell current and the cell temperature, as shown in Fig. 7. [42]

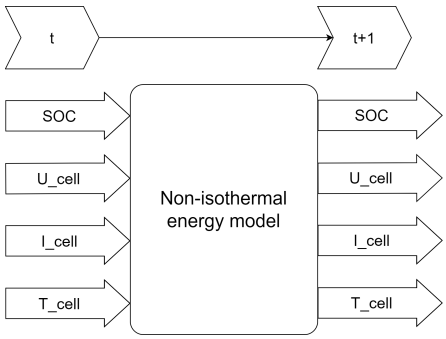

FIG 7. Scheme of the non-isothermal energy model

The model does not calculate the exact capacity required, but works with a database of selected commercially available battery packs. The reason for this is the need for information on actual electrical and mechanical parameters of the battery pack which have a direct influence on the calculation. These include the dimensions, mass, and maximum discharge current.

Internal resistance, OCV and thermal behavior

The data basis for the calculation of the values of the internal resistance calculator is taken from Soko Heli Tools Ltd. [43], which in turn uses a user database from the forum “RC Groups” [44]. This database includes measurement results of several hundred battery packs [44]. The open-circuit voltage (OCV) of a battery pack can be formulated as a function of the SOC. A data set comprising 34 battery packs is used for determining the OCV in the model [45]. The OCV is considered independently of the battery-cell temperature. Charge or discharge causes thermal heating of the cell. Heat-flow rates from the cell to the environment by conduction and convection are considered as well. In this case, however, thermal radiation is neglected. For simplification, a uniform heat distribution

in the cell and a location-independent cell temperature, which also defines the temperature of the entire battery pack, are assumed. The temperature of the cells corresponds to the ambient temperature at the beginning of the simulation.

3.5. Required energy and power

The model-based analysis of the battery size uses data sets from preliminary flight tests with a battery-electric multicopter with a take-off mass of 1.7 kg. Assuming that the power requirement of a multicopter for flight operation scales linearly with its mass, the electrical power obtained from the data sets is corrected according to the difference in mass. Four different scenarios are considered:

1) structure scan: flying around a fictitious obstacle (e.g., building or wind turbine),
2) standard: flying back and forth,
3) area scan: flying over an area in parallel linear flight trajectories, and
4) maximum: flying back and forth with maximum power.

For the analysis, the load profiles are scaled to about one hour of flight duration.

3.6. Simulation results

The simulation results are summarised in Fig. 8. A detailed explanation is given below.

Battery-electric flying

For a reserve flight duration of 3 minutes, the energy requirement for scenarios 1 to 3 is about 2.8 kWh (scenario 4: 3.2 kWh). The resulting mass of the battery would be 14 to 20 kg. Here, it becomes clear that a hydrogen-powered energy system can be a solution to save weight.

Fuel cell without operation management

Assuming that the fuel cell can provide its maximum power of 4.8 kW at all times and that the state of charge should be at least 5% at the end of the flight for safety reasons, the battery would not be required for scenarios 1 to 3, as the power demanded is always below the fuel-cell power. For scenario 4, this results in a battery with just under 300 Wh (mass: 1.64 kg).

Fuel cell with increase factor

Assuming that the fuel cell cannot or should not follow instantaneously the load power demand (e.g. to increase the service life), a variant of the implementation is examined in which the rate of fuel-cell power increase is limited, and additional power is provided by the battery. If the power increase is limited to 10% per second, this results in battery capacities in the range of 15-27 Wh (scenarios 1 to 3) and 650 Wh (scenario 4).

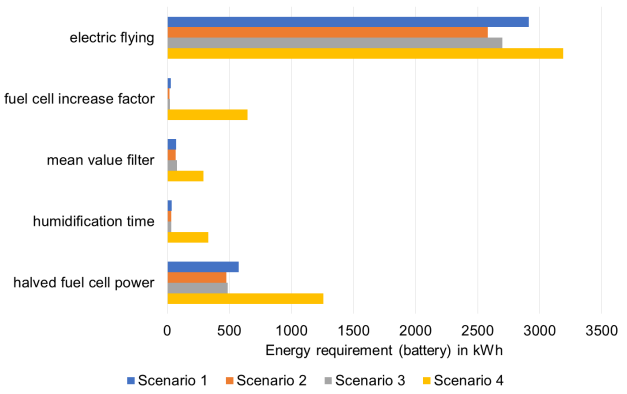

FIG 8. Battery capacity required for the scenarios

Mean value filter

Alternatively, battery capacities of 67-72 Wh (scenarios 1 to 3) and 290 Wh (scenario 4) are required when using a moving average filter (time span 20 seconds), which limits the fluctuations in the power output of the fuel cell.

Humidification time

The case where a fuel cell requires humidification every 20 seconds for 200 milliseconds, during which the power output is zero, is considered next. The battery alone must provide the power at the humidification time and must therefore be able to provide the significantly higher discharge currents during flight compared to a fuel cell without humidification. Instantaneous power adjustment of the fuel cell is assumed. Battery capacities of about 33 Wh are required for scenarios 1 to 3, and 328 Wh for scenario 4.

Halved fuel-cell power

Since the stack of the IE-SOAR 2.4 fuel-cell system has a nominal power of 2.4 kW and a mass of 4.8 kg [19], assuming that a stack with half the power has half the mass, the battery calculated may be 2.4 kg heavier compared to a scenario with a power of 4.8 kW without resulting in a disadvantage in terms of payload. This is a rather optimistic assumption, because the performance of a system does not scale linearly with its mass. A fuel cell with halved power would have a mass of more than 2.4 kg. If no operation management is considered for the fuel cell, this results in battery masses of 2.34 to 3.11 kg for scenarios 1 to 3 and 5.14 kg for scenario 4 (plus 3.5 kg compared to 4.8 kW fuel-cell power). In the case of scenarios 2 and 3, the mass reduction of the fuel cell exceeds the additional battery mass: the use of a smaller fuel cell can be advantageous here. For scenario 4 in particular, it appears that the use of a stack with a power of 4.8 kW makes sense. With power halved, a battery with an additional mass of just under 3.5 kg would become necessary. This is significantly more than the maximum mass saved by a smaller fuel cell.

Analysis at high ambient temperatures

All simulations considered so far result in a maximum battery temperature of 28 to 44 °C at the end of the flight, for an ambient temperature of 25 °C. Now, an ambient temperature of 40 °C is assumed. It is assumed that the battery temperature corresponds to the ambient temperature at the beginning of the flight. In addition, a halved fuel-cell power (2.4 kW) without operation management is assumed. The simulation yields that the cell temperatures during the flight would rise to 55 to 56 °C for scenarios 1 to 3 and to 74 °C for scenario 4. If cooling on two sides of the battery pack by passing air during flight is taken into account, the temperatures drop sharply even for low flow velocities. It is noticeable that for an increasing air velocity, the state of charge increases slightly towards the end of the flight. For example, for scenario 3 with $v = 1$ m/s this is an increase of 0.04%, which means that the SOC increases from 10.39% to 10.45% towards the end of the flight. This effect can be explained by the lower heat output to the environment at lower battery temperatures: if the temperature of the cell is lower, less energy is released into the environment. This difference remains in the battery and causes a higher SOC at the end. The effect is not particularly large because the temperature difference is not particularly high. Thus, for scenarios 1 to 3 with a temperature difference of about 10 °C ($v = 4$ m/s v. $v = 0$ m/s), the SOC increases by 0.08 to 0.11% towards the end of the flight. For scenario 4 with a temperature difference of 22.5 °C, the SOC rises by 0.76%.

3.7. Discussion of the energy-system design

When designing the energy system, close attention must be paid to the operating conditions, as the results are highly dependent on them. This applies both to the time-continuous power requirement, which must be provided by the desired flight manoeuvres, and to the ambient conditions of the battery. In addition to the ambient temperature, the specific installation location plays a central role, as this can significantly influence the heat exchange and, thus, the cell temperature. Depending on the operating conditions, the rated power of the fuel cell must also be adjusted in order to obtain an energy system that is as light as possible. Depending on the application, a smaller or larger stack may prove to be more favourable. For all the analyses presented, it is true that the critical conditions for the battery occur towards the end of the flight. The cell temperature increases over the duration of the flight and reaches its maximum value at the end of the simulation. The cell voltage and the SOC become critical at the end, especially under high loads. The only exception is the discharge current, which can be exceeded at any time. However, if the power demand remains similarly high throughout the flight time, the permissible discharge current is first exceeded at the end of the flight. This is caused by the cell voltage decreasing over time due to discharge, which leads to a higher cell current at the same power.

4. CONCLUSIONS

This paper presents the concept and design of a multicopter UAV and its hydrogen-powered fuel cell-based energy system, which was conducted as part of a student project. An initial sizing is conducted based on data available from the literature and UAV manufacturers, as well as fuel cell and battery manufacturers. The optimal energy system architecture is determined based on a reduced-order simulation model. Finally, selection criteria for suitable fuel-cell subsystems are provided.
Next steps comprise the manufacturing, assembly, and testing of the UAV. The testing will be carried out in three phases. First, the structural strength will be tested using static loads. Then, the functionality of the UAV will be evaluated in a sequence of ground tests, hovering tests, and free flight. Finally, the UAV and its energy system will undergo thorough in-flight performance measurements.
Future projects could, for example, consider the design of a pressurised air supply to increases the system power density, or alternative methods of cooling, as well as microturbine-based energy systems.

Contact address:

mimic@tfd.uni-hannover.de

ACKNOWLEDGEMENTS

We would like to acknowledge the funding by the Hannover Region under the grant “Förderung eines Wasserstoff-Reallabors für den Aufbau von Wasserstoff-Kompetenzen am Campus Maschinenbau (BDs 4642)”.
We would also like to acknowledge the funding by the Deutsche Forschungsgemeinschaft (DFG, German Research Foundation) under Germany´s Excellence Strategy EXC 2163/1 Sustainable and Energy Efficient Aviation Project ID 390881007.
We thank the Leibniz University Hannover IT Services (LUIS) for providing computational resources.
Furthermore, we would like to thank Prof. S. Kabelac (Institute of Thermodynamics), Prof. R. Hanke-Rauschenbach (Institute of Electric Power Systems), and Prof. J. R. Seume (Institute of Turbomachinery and Fluid Dynamics) for providing institutional resources and infrastructure at Leibniz University Hannover.
We also thank Manuel Chávez Ortega for proofreading the manuscript.

References

[1] F. F. Lizzio, E. Capello, and G. Guglieri. A Review of Consensus-based Multi-agent UAV Implementations. *Journal of Intelligent & Robotic Systems*, 106(43), 2022. ISSN: 1573-0409. DOI: 10.1007/s10846-022-01743-9.

[2] J. Apeland, D. G. Pavlou, and T. Hemmingsen. Sensitivity Study of Design Parameters for a Fuel Cell Powered Multirotor Drone. *Journal of Intelligent & Robotic Systems*, 102(6), 2021. ISSN: 1573-0409. DOI: 10.1007/s10846-021-01363-9.

[3] DJI. DJI Mavic 3 Pro Handbuch, 29.08.2023. https://dl.djicdn.com/downloads/DJI_Mavic_3_Pro/20230425/DJI_Mavic_3_Pro_User_Manual_DE.pdf.

[4] Yuneec. Specs Yuneec H520E/520, 29.08.2023. https://us.yuneec.com/h520-series/info/.

[5] Doosan Mobility Innovation. DS30W, 29.08.2023. https://www.doosanmobility.com/en/products/drone-ds30.

[6] H3 Dynamics. HYCOPTER Hydrogen Drone. https://www.h3dynamics.com/hycopter-hydrogen-powered-multi-rotor-drone.

[7] EnergyOr Technologies Inc. H2Quad 1000 Product Brochure - Version 1 1. http://www.energyor.com/static/template/eo/images/products/h2quad1000/EnergyOr%20H2Quad%201000%20Product%20Brochure%20-%20Version%201%201.pdf.

[8] J. Apeland, D. Pavlou, and T. Hemmingsen. Suitability Analysis of Implementing a Fuel Cell on a Multirotor Drone. *Journal of Aerospace Technology and Management*, (12), 2020. DOI: 10.5028/jatm.v12.1172.

[9] G. Strickert. Faktencheck Multikopter: Ähnlichkeiten und Unterschiede zu etablierten VTOL-Konfigurationen. Braunschweig, Germany, 2016.

[10] L. Kopmann. Konstruktion einer wasserstoffbetriebenen Multikopter-Drohne mit gegenläufigen Rotoren für industrielle Anwendungen, 2022. Student thesis. In German.

[11] G. Amri. Konstruktion einer wasserstoffbetriebenen Multikopter-Drohne für industrielle Anwendungen, 2022. Student thesis. In German.

[12] T-Motor. Antigravity MN8012 KV100 Specifications. Accessed August 2023. https://store.tmotor.com/goods-1130-Antigravity+MN8012+KV100.html.

[13] B. Wang, D. Zhao, W. Li, Z. Wang, Y. Huang, Y. You, and S. Becker. Current technologies and challenges of applying fuel cell hybrid propulsion systems in unmanned aerial vehicles. *Progress in Aerospace Sciences*, 116:100620, 2020.

[14] J. Apeland, D. Pavlou, and T. Hemmingsen. State-of-technology and barriers for adoption of fuel cell powered multirotor drones. In *2020 International Conference on Unmanned Aircraft Systems (ICUAS)*.

[15] A. L. Dicks and D. A. J. Rand. *Fuel Cell Systems Explained*. Wiley, 2018. ISBN: 9781118613528. DOI: 10.1002/9781118706992.

[16] Doosan Mobility. Powerpack Specifications. Accessed August 2023. https://www.doosanmobility.com/en/products/powerpack.

[17] H3 Dynamics. Aerostak Datasheets. Accessed August 2023. https://www.h3dynamics.com/hydrogen-fuel-cell-systems-for-air-mobility.

[18] Honeywell Aerospace. 1200U Specifications. Accessed August 2023. https://aerospace.honeywell.com/us/en/products-and-services/product/hardware-and-systems/honeywell-hydrogen-fuel-cell.

[19] Intelligent Energy. IE-SOAR 2.4 Datasheet. Accessed August 2023. https://www.intelligent-energy.com/our-products/ie-soar-fuel-cells-for-uavs/.

[20] Spectronik. Protium Fuel Cell Specifications. Accessed August 2023. https://www.spectronik.com/fuel-cell.

[21] L. Xu, Y. Huangfu, R. Ma, R. Xie, Z. Song, D. Zhao, Y. Yang, Y. Wang, and L. Xu. A Comprehensive Review on Fuel Cell UAV Key Technologies: Propulsion System, Management Strategy, and Design Procedure. *IEEE Transactions on Transportation Electrification*, 8(4):4118–4139, 2022. DOI: 10.1109/TTE.2022.3195272.

[22] A. Kabza. Fuel Cell Formulary. 2001.

[23] Q. Chen, G. Zhang, X. Zhang, C. Sun, K. Jiao, and Y. Wang. Thermal management of polymer electrolyte membrane fuel cells: A review of cooling methods, material properties, and durability. *Applied Energy*, 286:116496, 2021. ISSN: 03062619. DOI: 10.1016/j.apenergy.2021.116496.

[24] J. Lee, M. H. Gundu, N. Lee, K. Lim, S. W. Lee, S. S. Jang, J. Y. Kim, and H. Ju. Innovative cathode flow-field design for passive air-cooled polymer electrolyte membrane (PEM) fuel cell stacks. *International Journal of Hydrogen Energy*, 45(20):11704–11713, 2020. ISSN: 03603199. DOI: 10.1016/j.ijhydene.2019.07.128.

[25] R. Borup, J. Meyers, B. Pivovar, Y. S. Kim, R. Mukundan, N. Garland, D. Myers, M. Wilson, F. Garzon, D. Wood, P. Zelenay, K. More, K. Stroh, T. Zawodzinski, J. Boncella, J. E. McGrath, M. Inaba, K. Miyatake, M. Hori, K. Ota, Z. Ogumi, S. Miyata, A. Nishikata, Z. Siroma, Y. Uchimoto, K. Yasuda, K.-I. Kimijima, and N. Iwashita. Scientific aspects of polymer electrolyte fuel cell durability and degradation. *Chemical reviews*, 107(10):3904–3951, 2007. ISSN: 0009-2665. DOI: 10.1021/cr050182l.

[26] R. Singh, A. S. Oberoi, and T. Singh. Factors influencing the performance of PEM fuel cells: A review on performance parameters, water management, and cooling techniques. *International Journal of Energy Research*, 46(4):3810–3842, 2022. ISSN: 0363-907X. DOI: 10.1002/er.7437.

[27] C. Y. Ling, H. Cao, Y. Chen, M. Han, and E. Birgersson. Compact open cathode feed system for PEMFCs. *Applied Energy*, 164:670–675, 2016. ISSN: 03062619. DOI: 10.1016/j.apenergy.2015.12.012.

[28] A. Sorrentino, K. Sundmacher, and T. Vidakovic-Koch. Polymer Electrolyte Fuel Cell Degradation Mechanisms and Their Diagnosis by Frequency Response Analysis Methods: A Review. *Energies*, 13(21):5825, 2020. DOI: 10.3390/en13215825.

[29] H. Li, Y. Tang, Z. Wang, Z. Shi, S. Wu, D. Song, J. Zhang, K. Fatih, J. Zhang, H. Wang, Z. Liu, R. Abouatallah, and A. Mazza. A review of water flooding issues in the proton exchange membrane fuel cell. *Journal of Power Sources*, 178(1):103–117, 2008. ISSN: 03787753. DOI: 10.1016/j.jpowsour.2007.12.068.

[30] T. W. Patterson and R. M. Darling. Damage to the Cathode Catalyst of a PEM Fuel Cell Caused by Localized Fuel Starvation. *Electrochemical and Solid-State Letters*, 9(4):A183, 2006. ISSN: 10990062. DOI: 10.1149/1.2167930.

[31] M. L. Perry, T. Patterson, and C. Reiser. Systems Strategies to Mitigate Carbon Corrosion in Fuel Cells. *ECS Transactions*, 3(1):783–795, 2006. ISSN: 1938-5862. DOI: 10.1149/1.2356198.

[32] R. Herrendörfer, M. Cochet, and J. O. Schumacher. Simulation of Mass and Heat Transfer in an Evaporatively Cooled PEM Fuel Cell. *Energies*, 15(8):2734, 2022. DOI: 10.3390/en15082734.

[33] S. Toghyani, S. A. Atyabi, and X. Gao. Enhancing the Specific Power of a PEM Fuel Cell Powered UAV with a Novel Bean-Shaped Flow Field. *Energies*, 14(9):2494, 2021. DOI: 10.3390/en14092494.

[34] M. Käbisch, J. Teichert, C.and Haubrock, Z.A. Styczynski, and A. Lindemann. Energiemanagement für Brennstoffzellensysteme in Fahrzeugen. 2007.

[35] A. Brinner and P. Treffinger. Energiemanagement von Brennstoffzellenantrieben. Technical report, Deutsches Zentrum für Luft- und Raumfahrttechnik e.V. (DLR), Stuttgart, Germany, 2001. In German.

[36] J.M. Tarascon and M. Armand. Issues and Challenges Facing Rechargeable Lithium Batteries. *Nature*, 414, December 2001. DOI: 10.1038/35104644.

[37] S.-J. Kwon, S.-E. Lee, J.-H. Lim, J. Choi, and J. Kim. Performance and Life Degradation Characteristics Analysis of NCM LIB for BESS. *electronics*, December 2018.

[38] R. Rahimzei, K. Sann, and M. Vogel. Kompendium: Li-Ionen-Batterien, July 2015.

[39] L. Kistner, A. Bensmann, and R. Hanke-Rauschenbach. Optimal Design of Power Gradient Limited Solid Oxide Fuel Cell Systems with Hybrid Storage Support for Ship Applications. 2021. DOI: 10.1016/j.enconman.2021.114396.

[40] F. V. Conte. Battery and battery management for hybrid electric vehicles: a review, September 2006. DOI: 10.1007/s00502-006-0383-6.

[41] Harding Energy Inc. Harding Battery Handbook For Quest® Rechargeable Cells and Battery Packs.

[42] X. Lui, Chen Z., C. Zhang, and J. Wu. A novel temperature-compensated model for Li-ion batteries with dual-particle-filter state of charge estimation. 2014. DOI: 10.1016/j.apenergy.2014.02.072.

[43] Soko Heli Tools Ltd. Lipo Calculator. https://www.soko-heli-tools.com/calculators?tab=lipo-calculator.

[44] RC Groups. The Lipoly Objective Performance Database. https://www.rcgroups.com/forums/showthread.php?1578001-The-Lipoly-Objective-Performance-Database.

[45] B. Pattipati, B. Balasingam, G. V. Avvari, K. R. Pattipati, and Y. Bar-Shalom. Open circuit voltage characterization of lithium-ion batteries.